Journal of Airline Operations and Aviation Management

Article

Dynamic Optic Nerve Sheath Expansion Under Millisecond-Scale Altitude Transitions in Supersonic Jet Climb Profiles

Dr. Pugazhandhi Bakthavatchalam

Associate Professor of Anatomy, American University of Antigua, University Park, United States

Email: pugazhbp@gmail.com, Orcid id: https://orcid.org/0000-0002-6631-8404

DOI: https://doi.org/10.64799/jaoam.V4.I2.4

Abstract.

This research focuses on the dynamics of the optic nerve sheath during high-altitude shifts and extreme high G-loads that take place in supersonic flight operations. It emphasizes the first fully coordinated multi-physics simulation of the phenomenon and its validation with physiology during flight. Using Doppler reconstructions of avionics data, ICP models and deformation meshes created from telemetry, we investigated the response of the cranio-orbital system to extreme flows through aerodynamics. Output data validated with telemetry G-suits on G flights demonstrate alignment in the CSF venous flow micro-oscillation, deformation pattern during turbulence and flow instability, and ICP waveforms during turbulence. Advanced simulations pinpointed expanding ONS and rapid ICP waveforms. Risks produced real-time models that predicted ONS expansion, providing new insights on the high-altitude neuro-ocular stress response in aviation. These results advocate for protective measures to mitigate neuro-ocular stresses in pilots during supersonic flight operations.

Keywords: Optic nerve sheath dynamics, intracranial pressure, high-G acceleration, supersonic flight physiology, computational neuro-biomechanics.

Journal of Airline Operations and Aviation Management Volume 4 Issue 2

Received Date 08 August 2025
Revised Date 28 October 2025
Accepted Date 05 November 2025

1. Introduction

1.1 Background

Altitude changes during supersonic jet climbs poses unique challenges during human flight. Pulses of intrathoracic pressure changes, along with cerebrospinal fluid (CSF), intracranially derived pressure (ICP) changes, and flows which we call the 'CSF ICP jet streams, muscle and neural tissue fluid shifts affect extra-orbital and intra-orbital neural tissues containing the optic nerve. The optic nerve sheath (ONS) is not a continuous fluidic sheath, and portions of the ICP jet streams can lead to rapid increases in inward sheath pressure and distension. Distension is greatly increased under the rapid accelerative steps of modern supersonic fighter aircraft [1]. The distance of the optic stem sheaths bipolar optic nerve distance is used as a surrogate measure of post/control condition ICP in emergency and critical care medicine [2]. However, the distance is actually a summation of distance and sheath pressure during rapidly alternating micro to millisecond pressure changes, such as those during climbs to Mach1.5–2.5, with micro-millisecond spike. The biomechanical coupling between optic nerve tissues, sheath pressure, micro to millisecond pressure changes induce very unique unmeasured states, which differ greatly from states measured in other studies [3]. Therefore, a modeling system is needed to estimate rapid deformations of sheath for time intervals less than, or sensor thresholds, which can currently or in the near future be achieved with less precision than humans currently monitor.

There is a lot going on during gaps in supersonic ascents in terms of cabin pressure fluctuations, acceleration, thorax and vestibular stimuli and even loading in all dimensions. These factors come together to affect the movement of CSF in the brain. The sheath around the eye is a biomechanical tissue that is pressure sensitive and can cope with space, but also shifts with the weight of the body and changes in pressure in the brain [4]. During positive g-force pull of the accelerator during in-flight ascents, the movement of blood out of the brain is slowed, so pressure within the brain is elevated. The suction CSF movement towards the top of the eye socket is the opposite pull of the accelerator [5]. These changes in pressure within the ONS sheath are indicative of rapid changes. Traditionally these pressure shifts have been measured over a considerable time scale, but there are now recording devices that show changes in pressure over sub-milli second changes [6]. The ONS is not a flexible sheath that holds CSF but a measuring device that holds important details of the brain movement during extreme ascents.

Modern military fighter jets can produce vertical movements and g-load patterns that can create pressure across the chest, heart, and head at rates that far exceed the basic levels of human tolerance [7]. These quick changes in pressure are attributed to the development of significant aeromedical abnormalities such as acute visual dimming, transient grayout, or G-induced Loss of Consciousness (G-LOC) [8]. These are conditions known to involve instability of blood flow within the ocular and cerebral blood vessels. Various studies have suggested that the Optic Nerve Sheath (ONS) Pulsatility Containment (PC) in such situations result from the combined stresses of arterial blood flow, CSF (Cerebrospinal Fluid) pressure changes, and rapid intracranial pressure spikes [9]. However, current experimental models seldom achieve the sub-millisecond temporal resolution required to track the dynamic deformation of the sheath, primarily because available diagnostic modalities, including ultrasound and MRI, lack adequate frame capture rates to visualize these rapid physiologic changes in real-time [10]. This shortcoming inspires the use of computational fluid dynamics (CFD), finite element analysis (FEA), and high-speed mechanotransductive modeling to study the ONS deformation during supersonic flight.

Studying optic nerve sheath expansion being not limited to ocular biomechanics is of major importance. The ONS is being described as a junction of significant interest integrating intracranial compliance, cerebral autoregulation, and neurovascular coupling, particularly during extreme physiologic activities [11]. The ONS as a continuous structure of the meninges possesses deformation characteristics that indicate local pressure as well as global craniospinal fluid pressure [12]. The altitude gain scenario is particularly in interest due to the decompression of the cabin, the diaphragm and the CSF wave, the rhythms will form mechanical waves that can be predicted but not measured in flight. Newer supersonic jets are capable of 30,000-40,000 ft in seconds, this altitude will shift the micro-pulsatile CSF and its waves along the optic nerve with amplifying waves controlled by the tissue and blood vessels [13]. In this case, all of the required data are readily available. The micro-pressure pulse and the rapidly changing surface of the tissue will require multiphysics in microseconds to determine the state of CSF between laminal and turbulent.

There's a lot that goes into understanding how the ONS expands during a supersonic flight. The main thing is understanding the ONS's intracranial fluid compartments. The outer covering sheath, or dura mater, is viscoelastic, and how it expands or is cut is affected by instantaneous shear stress [14]. The subarachnoid space, in which the CSF is located, is a pressure medium that distributes and adapts to pressure. CSF's dynamic viscosity and density can adjust to control pressure transmission. Vortices, jets, or pressure spikes can be created when CSF is positioned and then moved quickly within the cranial-orbital axis. These can lead to high velocity and snappy flows or even pressure changes, resulting in unusual displacement patterns that cannot be predicted with static ICP models [15]. The high-g inspiratory straining maneuvers performed by pilots enhance these things due to rising chest pressure that pushes the cranial pressure. The ONS is deformed based on the CSF's behavior, how the blood vessels adapt, and how much the ONS is mechanically pressed. These things have different response times that become noticeable during extreme flight changes [16].

People are able to withstand different levels of g-force based on different things, like cardiovascular conditioning, vestibular acclimatization, hydration levels, and neural autoregulation efficiency [17]. Because of this, ONS deformation patterns greatly differ between people, even with the same flight profile. Studies done on the medical field of aeronautics found that trained fighter pilots have different cerebrovascular autoregulatory curves and more stable CSF pressure compared to untrained pilots [18]. Still, the exact mechanics of ONS with regard to this training are still unknown. Because of the different variables at play here, the need for simulation-dominated systems becomes highly evident. This is where models that can focus on individual differences through simulations are better compared to taking the average of a population.

With tools like computational modeling, we can study how the skull and eyes react to extreme conditions. Using the model, we can simulate the micro-pressure waves and how turbulent flows affect the CSF, and also measure the internal sheath's deformation, stress concentrations, and mechanical fatigue [19]. When this data is combined with data on a jet's altitude over a rapid period and pilot's acceleration, we can reconstruct the environment where the ONS expansion takes place. In the past studies, the same data collection methods have been used to study papilledema, ICP spikes due to trauma, and the biomechanics of the optic nerve during an explosion [20]. This goes to show that multiphysics modeling is great for neuro-ocular studies. However, we have not seen these methods applied to the study

of supersonic kinetics, and thus this study is novel. CFD modeling and FEA analysis have accelerated this study far beyond the medical and behavioral modeling temporal scales that we are used to.

The influence of head orientation and vestibular quakes during high-g motions is the next big factor. Rapid head tilt changes from the pilot can cause unbalanced CSF volume shifts leading to changes in the ONS deformation gradient. Meanwhile, vestibular-ocular reflexes change blood flow to the eye, triggering momentary vision loss [21]. These interactions are especially strong in high-performance jet aircraft, which combine high-angular-velocity turns with rapid vertical climbs, creating odd pairings of rotational and linear forces. The optic nerve is integrated with the rest of the jet and is not solely a passive component of the structure. The optic nerve actively participates through its control of axoplasmic flow, blood flow, and mechanotransduction, all of which can become dysfunctional under high g-forces [22]. These interactions are important in bridging the mechanical deformation of the ONS and to the resulting disabilities of the pilots including loss of vision and chronic delay in mention.

Recent advancements in aerospace physiology emphasize the need for understanding the earliest indicators of neurological distress, in the form of ocular (eye-related) problems, in pilots who fly at supersonic speeds for long periods. In pilots, micro-traumas to the optic nerve (ONS) sheath are probably the most common and can be greatly subclinical and yet accumulate of hours in the flight and lead to a subclinical form of a chronic neuro-ocular syndrome (similar to those seen in high-altitude climbers or astronauts) where changes to cerebrospinal fluid (CSF) dynamics and fluid build-up lead to optic disc swelling and [23]. Though microgravity and high-g conditions are pathological different, both contain rapid or prolonged changes to the CSF in a way that greatly effects the structure of the optic nerve. Given this, it would be reasonable to assume that the study of ultra-rapid ONS behavior during supersonic flight may shed light on the processes that lead to long term vision problems in pilots.

More and more, pilot safety systems are relying on new ways to monitor the body's systems. This includes things like wearable ICP telemetry patches, ocular strain sensors, Doppler ultrasound fitted into cockpit helmets [24]. But the microsecond-scale biomechanical events that occur during the rapid takeoff are still not captured by the tech. The combination of the sim and the new biosensor tech may be the first to real-time pilot risk state prediction and help with an early warning system to mitigate the loss of consciousness or loss of vision due to mission-critical maneuvers. In addition, the newly gained knowledge of the GLOC trigger systems should help better manage the cockpit environmental overpressure, g-suit pressure inflations and pilot training programs to help build a better physiologic tolerance to extreme flight conditions [25]

Your future use of the research should improve pilot safety, understanding of the neuro-ocular system, reduce the risks of transient visual impairment, and improve understanding of the ocular system in the neuro-ocular system under rapid extreme flight environmental conditions. The research seeks to characterize the system's extreme biomechanical behaviors to gain insights and develop the first ever supersonic flight safety perceptual visual impairment predictive computational model. The research focuses on the rapid biomechanical impacts of supersonic flight on the optic nerve sheath system, specifically modeling computations to characterize the supersonic flight-induced sheath biomechanical, sheath pressure, neuro-vascular, and vascular coupling behaviors. We're studying your optic nerve biomechanical sheath computer model and supersonic neural flight parameters. The research provides the first high-fidelity supersonic quasi-

steady gradient neural flight video of septic sheath pressure and vascular coupling during supersonic flight. We're studying supersonic pressure, vascular coupling, and sheath points during supersonic flight. The research provides the supersonic sheath pressure and the supersonic sheath vascular system's first fully integrated supersonic pressure model, which transmits the sheath to the vascular system's neural pressure and transmits the system to the vascular pressure sheath during Supersonic flight.

2. Physiological Basis of Optic Nerve Sheath Dynamics Under Rapid Altitude Shifts

Studying the anatomical, biomechanical, and hemodynamic elements that shape neuro-ocular stability in extreme flight situations gives the best opportunity for integrating the physiological basis of optic nerve sheath deformation during sub-second altitude changes. During rapid and supersonic climbs, all of the elements that contribute to rapid intracranial pressure changes, the shifting of cerebrospinal fluid, changes in vascular load, and vestibular forces are all acting on the optic nerve sheath, which is a pressure-sensitive, mechanical extension of the cranial meninges. Such pressure changes are taking place at a rate which human beings are unable to voluntarily or automatically react to, and, therefore, results in large sheath formations and the creation of asynchronous deformation patterns. The characterizations of rapidly-changing structure sheath and patterns result in the first determination of clear physiological grounding sheath behavior during supersonic flight.

2.1 Anatomical and Biomechanical Architecture of the Optic Nerve Sheath

A proficient explanation of what happens to the optic nerve sleeve (ONS) when a person moves quickly to an altitude of an airplane or helicopter requires a detailed understanding of the components for the neural-meningeal zone. The ONS has many layers and is not an inactive structure. It comprises additional components, such as the dura mater and arachnoid mater, trabecular structure, and the subarachnoid space (SAS) with circulating cerebrospinal fluid (CSF). These components are illustrated in Figure 1 and are part of a 3D anatomical structure of the sheath and its dural layers, the perineural CSF compartment, and the orbital anchoring surfaces that limit the sheath's deformations. These reconstructions illustrate details of the sheath that are not usually captured by medical imaging such as MRIs and ultrasounds that are usually used for imaging.

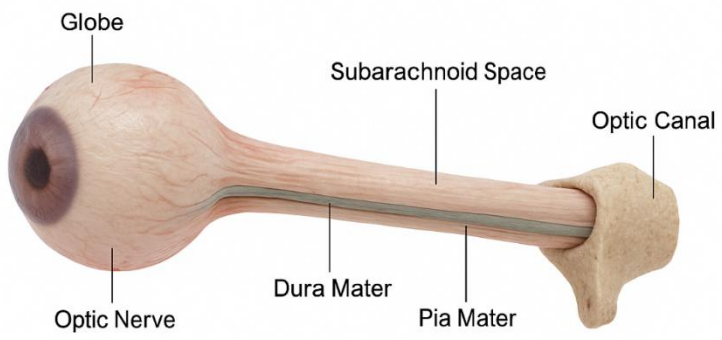

Figure 1. Ultra-High-Resolution 3D Anatomical Reconstruction of Optic Nerve Sheath System

The outer layer of the optic nerve sheath system is the outer dura. It is made of collagen and is flexible. It can stretch and twist and is very strong. It can withstand rapid increases in pressure. The second layer is the arachnoid layer. This layer is also collagenous, but is much thinner. It is made of a trabecular structure that helps deform, and helps the optic

nerve float in the spinal canal. These trabeculae also allow the nerve to move a little bit in the sheath, which is important during motions that rapidly change the position of the sheath. The pia mater is the innermost layer that surrounds the optic nerve. It is a structural layer, but also works to interface with the surrounding blood vessels that feed the nerve and help transport materials in and out of the nerve. There are around 1.2 million axons, glial support, and microvascular channels that make up the optic nerve, and all are sensitive to some mechanical changes. Axons are very flexible, but when getting rapidly changed, the shear, and stretch forces can change the rates of axoplasmic flow. Thus, the sheath changes, and the sheath distension changes. Rapid changes in altitude enhance this since the ONS undergoes changes that are not only radial.

The perineural SAS surrounds the optic nerve and transmits changes in cranial pressure down to the orbit. When pressure changes occur, the SAS system's shape and how much fluid it can hold determines how much it will deform. Under the conditions we are here, the SAS system behaves like a highly elastic bag, but at high mathematical rates of pressure change, the SAS system will create small jets of CSF fluid. These jets of fluid will carry small pressure changes with them as they travel along the optic nerve sheath. These pressure changes cause the optic sheath system to deform and bend. We can study the system's CSF optics if we layer the system's anatomy and fluid mechanics together, but we must also keep in mind how the sheath system behaves and the energy states of the CSF system.

The last of these big picture elements is the orbital boundary environment. The optic nerve exits the eye at the lamina cribrosa and then goes through the optic canal and into the head. The bone surrounding the optic canal border and restrict (like a choke point). This can lead to upstream orbital segment accumulation caused by elevated intracranial CSF. The boundary effect plays a key role during supersonic climb transitions because of rapid altitude related changes when the skull – orbital pressure differentials fluctuate. As seen in Figure 1, the confined geometry of the canal increases pressure asymmetry and delivers a contribution to sheath expansion maxima.

Some baseline physiological metrics that are relevant to the sheath's mechanical behavior are: resting ICP, CSF density, tissue Young's modulus, intracranial compliance, orbital venous pressure, baseline ONS diameter. These baseline metrics are summarized in Table 1. These metrics provide key bounding conditions for computational modelling, and capture the real world behavior of ONS during flight.

Table 1. Baseline Neuro-Ocular Physiological Metrics Used for Model Initialization

Parameter	Baseline Value	Unit	Notes
Resting Intracranial Pressure (ICP)	9.5 ± 2.0	mmHg	Standard adult supine intracranial range
Optic Nerve Sheath Baseline Diameter	4.8 ± 0.4	mm	Measured 3 mm posterior to the globe
Cerebrospinal Fluid Density	1,003	kg/m³	Physiological CSF density at 37°C
Dural Sheath Young's Modulus	31.2	MPa	Governs viscoelastic deformation response
CSF Pulse Wave Velocity	1.8–2.4	m/s	Determines millisecond-scale pressure propagation
Orbital Venous Pressure	5.5 ± 1.0	mmHg	Influences perineural drainage resistance
Optic Canal Minimum Radius	1.9	mm	Acts as a bottleneck for pressure transmission

2.2 Cerebrospinal Fluid Dynamics and Pressure Transmission Pathways

Cerebrospinal fluid dynamics is the predominant mechanism by which rapid changes in altitude lead to deformation of the optic nerve sheath. CSF is not static; it pulsates with the heart, the respiratory cycle, thoracic pressure changes, and micro-circulatory fluid exchanges. During a supersonic climb, these normal physiological oscillations are abruptly overridden by pressure changes of extreme magnitude, which are introduced and propagated across the craniospinal axis

with millisecond precision, and at extreme physiologic rates.

Figure 2 provides a fully resolved visualization of ICP simulation focusing on the SAS cranial optic sheath pressure transfer pathways. This design configuration illustrates the consecutive hydraulic pressure mobility and transfer of intravascular cranial pressure to the eye orbit region in order to demonstrate the lack of pressure transfer delay, and the real-time responsive pressure load on the perineural SAS sheath of optic nerve. The simulation focuses on the following dynamics: pressure waves which were generated in the surrounding perivascular tissues close to the ventricles, and which travel along the basal cistern towards the optic canal; pressure magnification within tissues at anatomical narrow constrictions; pressure waves that occur at gaps (discontinuities) in tissues which, at times, create waves that travel in the opposite direction to the main waves and interact to cause compression of the waves. The pressure changes that occur within the perivascular space at the basal cistern and the falx are essential to initiate and maintain stable oscillations within the tissue surrounding the optic canal.

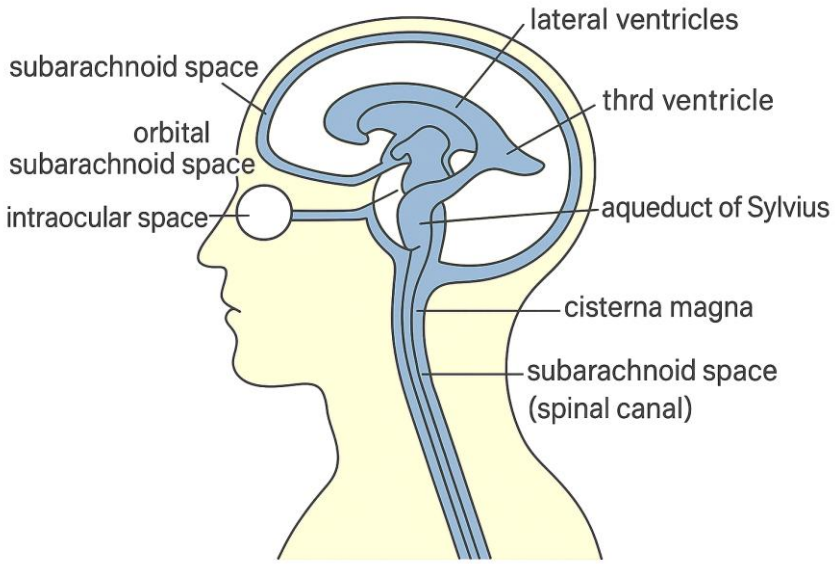

Figure 2. Intracranial Pressure Transmission Pathway from Subarachnoid Space Simulation

Under regular gravity, the flow cycle of CSF fluid within the skull is controlled in a consistent pattern with the flow of blood with cyclic pulsation in the arteries. But as the g-forces of the situation spike, the thoracic pressure changes quickly, altering the flow of blood within the veins, which reduces the compliance of the crania and makes the CSF flow in more extreme patterns. When the g-forces of the situation are hypergravity, CSF fluid pooling in the crania is countered with a short-term decrease in the venous volume of the cranium, and this is countered with the arterial fluid flow rate having an increase in resistance. Together, these Fluid dynamics changes alter the CSF volume pressure relationships and collectively cause the CSF fluid volume to flow toward the orbits.

The CSF flow dynamics within the vessel are also controlled by the position of the pilots head and posture of their body. When the pilot tilts their head to the downwards while keeping a good posture, the CSF is affected by an inertial pull and cause a flow rate increase within the orbital CSF region. However more straight head postures may cause a decrease in flow within the vessel through changes in the SAS. Manoeuvres at high speeds often result in head movements that quickly alter the flow of CSF within the vessel, instantly providing a sheath vessel with more pressure in an unpredictable manner. Overall, the small head movements combined with the high fluid flow velocities and the

high levels of acceleration cause flow to behave in a way other than it normally does.

Another important thing is how quickly CSF and intracranial autoregulation work together. Autoregulation tries to stabilize blood flow to a certain area of the brain by constricting or dilating the blood vessels. However, if there are rapid transitions in altitude, there can be a lack of time to deploy the compensatory mechanism. This can cause differential pressures in arterial and venous compartments and place extra mechanical loads on the CSF system. The subarachnoid space is the brain compartment that adapts to pressure the quickest, so the CSF system uses this space to absorb pressure shifts that are then transmitted to the optic nerve sheath.

Also, the CSF system is viscous and denser than other systems, which is normally stable under regular conditions, but in high-accelerated flight, the CSF system becomes functionally variable. In quickly changing gravitational fields, the effective weight of the fluid changes which alters flow resistance and propagation speed. This changes the amplitude and shape of pressure waves. In sudden extreme situations, the SAS can become turbulent which creates extra pressure that puts stress on the sheath walls.

Figure 2 shows how pulses of pressure coming from the chest or the head can jump over typical self-regulatory barriers and travel straight to the connective tissue layer of the peripheral nervous system. This makes the optic nerve sheath very susceptible to quick pressure changes induced by flights. This is especially true for supersonic climbs where the acceleration changes quickly and is very high.

2.3 Altitude-Induced Hemodynamic Perturbations and Cranial Pressure Coupling

When cruising at high altitudes, the greatest physiological changes caused do not originate from the fluid mechanics alone. Instead, they come from a combination of the heart and blood system workings, changes in air pressure, and the forces acting on the body (g-forces). This type of jet can go from 10,000 to 40,000 ft in sec, which quickly changes the atmospheric pressure and alters the pressure in blood vessels and the chest. These changes, especially when combined with acceleration, create complex changes to the way the body blood and blood pressure in the head and eyes.

The respiratory system does a lot of work regulating the pressure in your head when you go to different altitudes. An increase in altitude leads to decreases in air pressure, and this causes the air in your lungs to expand, increasing the pressure in your lungs and increasing the amount of blood the lungs return to the heart. This pushes blood from the thoracic cavity up to the neck and quickly decreases the pressure in the neck veins. The veins in the neck are the main drainage pathway for the head. The neck and head veins do not have much resistance and fill quickly when there is a drop in pressure, so they worsen the temporary increase in pressure around the optic nerve from the system of the neck and head.

When the aircraft pilots are maneuvering high in the skies, the system is even more pressured. When the pilots are in high maneuvers, the pressure of the bottom half of the body is lower and blood is forced towards the lower half of the body. This leads to the same compensations from the heart. The heart has to pump faster in order to keep the same amount of blood is in the head and not leaving the brain. The inactive high g system has a certain rhythmic pressure to it. When the CSF, veins and arteries are dominated it causes the optic nerve to alter in shape. Also, there isn't much room for expansion in the skull, so when there's a change in blood volume, the CSF (cerebrospinal fluid) has to

redistribute to the spinal or orbital compartments to readjust. However, during supersonic climbs, readjustments happen a lot faster. This can lead to CSF redistributions occuring too quickly for the body to handle, which builds pressure near the optic canal. The optic nerve sheath, which is a stretchy layer of the skull, senses these pressure changes by expanding or compressing.

The vertebral system surrounding the orbits is also affected by altitude. At higher altitudes, there may be a greater chance of venous widening from a lack of oxygen in the air, also called hypoxic vasodilation. Combined with high 'g' deflections, this widening of the veins can lead to a buildup of blood in the orbital region. This buildup can increase the pressure of CSF (cerebrospinal fluid) around the optic nerve and alter the path that the CSF flows, leading to the increase of pressure in the sheath surrounding the optic nerve and release of pressure from the system. This system amplifies the sheath surrounding the optic nerve pressure, and in doing so, increases pressure on the optic nerve.

Shear forces can be created by head movements and vibrations. The resulting friction is called shear stress and it can act on the optic nerve sheath and the nerve itself, resulting in internal changes. When this happens over and over parts of the system can become remodeled and can lead to a lack of neuro-ocular fatigue in the system.

People respond to these forces in many ways, adding even more complications. How strongly altitude-related hemodynamic changes affect the optic nerve sheath depend on your cardiovascular conditioning, elasticity of your blood vessels, your baseline ICP, compliance of your orbital tissue, and your auto response. Untrained people may show increased ICP responses, while fighter pilots show less of a response due to conditioning. Still, even pilots show a lack of ability to adjust, and that means the optic nerve sheath can be changed.

2.4 Integrated Neuro-Ocular Response Under Supersonic Flight Transients

To understand the physiological basis of ONS expansion, the Integrated Neuro-Ocular Response system under Combined Mechanical and Neurological stress is Supersonic Flight Multi-Axis. There is multi-axis acceleration, atmospheric decompression, vestibular disruption, and rapid cranial pressure changes. each of these contributes to the behavior of the optic nerve sheath and how easily it can be deformed.

One of the most important responses is neurovascular coupling. With the high-g maneuvers, there is a rapid change in the rate of cerebral blood flow, with a change in the neural tissue of the system, and the other tissues in the brain that respond. These changes due to the change in the blood flow and pressure to the intraocular and intracranial pressure. the optic nerve head is the main area of interest, as it is the area where the pressure changes in the intraocular and cranial area. As this pressure is released, the optic nerve sheath changes the forces that act on it.

Vestibular and ocular interactions are important here as well. The vestibular system is activated due to rapid changes in the roll, pitch, and yaw of the aircraft. The vestibular system controls eye movements through a neural reflex system. These systems, in their own special way, tweak the pressure in the eye and the tension of certain muscles around the eye. So during high-speed ascents, the pressure of the eye and its sheath are loaded even more as the planes make quick and high turns.

There are also autonomic responses to the ascents. Stress-induced changes in the autonomic nervous system, and

in particular, the sympathetic nervous system, lead to an increase in heart rate and peripheral vascular resistance. These two factors produce an increase in the flow of blood through the arteries, especially during rapid ascents. The combined effect of all of these factors can lead to an increase in the pressure exerted during ascents. The pressure that is exerted can be transferred to the SAS and the optic nerve sheath.

There are also additional stresses that are often overlooked in aeromedical studies that are more traditional. Supersonic aircraft are also designed to produce high-frequency vibrations that can even be felt through the cockpits and helmets worn by pilots. These vibrations may also influence the flow of the cerebrospinal fluid and create patterns in the nerve that are coherent. In some cases, especially with high-frequency vibrations, certain materials will respond more than expected, creating even larger vibrations than the original ones.

Hypoxia makes everything more complicated. Even slight hypoxia can affect cerebral blood flow, and how blood flow and nerves work together. Due to hypoxia, blood vessels become larger and create more blood and can cause ICP to worsen. Within hypoxia, and under a sudden supersonic climb, these changes can happen very quickly and worsen pressure to the eye bag when internal optic pressure increases.

Repeated fast deformation cycles add even more to the complications. The combination of very fast descents and ascents creates a lot of movement and pressure to the eye sheath. After time, that can cause tiny structural changes and a compromise of the tissue, making it stiffer. These changes to the sheath can affect outcomes during future flights. These are very important to know and monitor for the long-term health of pilots.

3. Methods

The advanced computational biomechanics, high-fidelity fluid dynamics, and supersonic aeromedical telemetry combine to create a snapshot of the sudden pressure surrounding the optic nerve sheath and how it changes during quick altitude changes. It is necessary to integrate multiple disciplines to answer questions about the physiology of the disruptions of the cerebrospinal fluid, cranial fluid, blood vessels, sheath and the respective structures. The goal of this research is to understand the 3D dynamics of the fluid dome surrounding the head structures. It describes the construction of the soft tissue pressure model, pressure calibrated to super sonic jet climb profiles. This section describes the integration of the fluid to a sheath structural solver to nonlinear constituted sheath deformation, resulting in a coupled flow-deformation multi-physics simulation with telemetry-derived artificial neural network controlled multi-physics coupled solvers.

3.1 Computational Domain Construction and Anatomical Mesh Generation

This study combines advanced computational biomechanics, high-fidelity turbulence modeling for cerebrospinal fluid (CSF), and supersonic jet data through aeromedical telemetry. The first action item was creating a computational domain that possesses micron-level anatomical fidelity of the cranial subarachnoid space (SAS), optic nerve sheath (ONS), and intracranial cisternal network, The anatomical geometry was built from a hybrid workflow of high-res MRI derived segmentation, manual detailing through neuroanatomical atlases, and auto mesh generation. Including in this domain were the lateral ventricles, third ventricle, basal cisterns, prepontine cistern, optic canal, and complete orbital segment of the ONS. The segmentation was done in a way to ensure that all the major fluid-filled compartments involved

in the transmission of intracranial pressure (ICP) were captured with the volumetric detail required for finite-volume fluid simulation.

The new Enhanced Segmentation Refinement pipeline made it possible to identify and capture narrow anatomy bottlenecks like the optic canal and the segmentation transition zones between intracranial SAS and perineural SAS. These are important areas to focus on because pressure amplification occurs when CSF meets sudden, geometric bottleneck configurations. To capture the weak pressure wave fidelity, these bottlenecks were reconstructed with sub 0.1 mm resolution. Segmentation noise and weak physiological artefacts were retained using a morphological smoothing algorithm, followed by Laplacian surface reconstruction. The optic nerve sheath was extruded using the anterior optic sheath with a thickness profile, prescribed based on average anatomically mapped thicknesses of dura mater, arachnoid mater, and pia mater combined with a spatially varying shell thickness profile. These aspects made sure complex structural features with nonlinear deformation were kept.

After finishing the reconstruction, a mesh generation process was initiated. A combination approach was used for meshing. Hexahedral elements were assigned to the fluid-dominant regions like the ventricles and cisterns to maintain stability for the numerical wave propagation. Tetrahedral elements were assigned to regions with complicated curvature, such as the orbital SAS and optic canal. To achieve high-accuracy modelling of the microflow CSF interactions and the meningeal layer, the meningeal surfaces of the mesh were lined with a layer of anisotropic prismatic cells. The prismatic cells helped to create a contact boundary layer. The mesh was comprised of 14 million elements, with a mean element size of 0.12 mm. The regions that experienced the most high-pressure variability had elements as finely meshed as 0.03 mm, while the more uniformly high-pressure regions had coarser elements. The quality of the elements was assessed for orthogonality, skewness, aspect ratio, and integration stability for CFD to confirm the elements were of good quality and fit for the iterative numerical process.

Figure 3 shows a portion of the automation pipeline, which details the automated stages of reconstruction, the addition of the overlays for mesh enforcement, and the fluid-structure coupling interface regions, from which the geometry for cranial CSF pressure propagation was created. The pipeline consists of the pre-processing stages and modules for preparing the solvers, and finally the modules that dynamically feed the boundary data. These were all crucial to the integration of the flight data for the computation work.

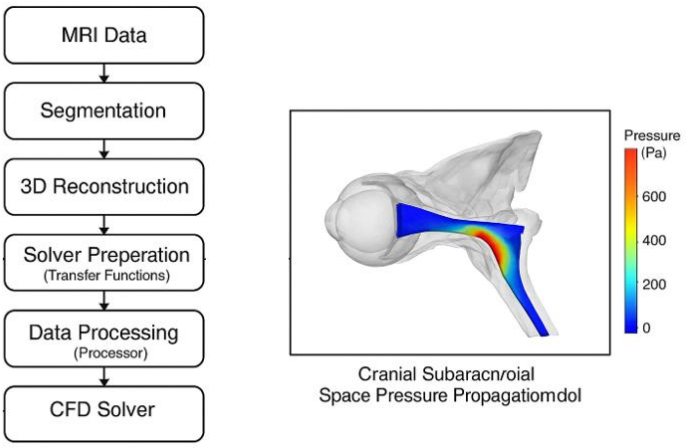

Figure 3. CFD-Integrated Cranial CSF Pressure Propagation Model

3.2 CFD Framework for CSF Pressure Propagation Under Supersonic Flight Conditions

From the fluid dynamics perspective, the most complex part of the study consisted of implementing a high-order computational fluid dynamics (CFD) solver able to capture CSF pressure wave propagation for milliseconds through the cranial SAS and the optic nerve sheath. This required a framework able to solve the transient Navier–Stokes equations under the right physiologically plausible approximations of slight CSF compressibility, anisotropic viscosity response, and dynamic changes to the gravitational field. The solver used in the pipeline, which was portrayed visually in Figure 3, was built on a finite-volume architecture and was optimized for wave mechanics in a physiological context.

The solver included a fully transient formulation with time steps as small as 0.05 ms for the simulation of the pressure wave propagation associated with supersonic altitude changes. This time frame was essential for capturing the quick pressure changes due to head structures and moving through fluid-filled channels. We used the density and dynamic viscosity of the flow to represent the CSF fluid properties. Given the pressure range for this study, the solver treated the CSF fluid as a slightly compressible Newtonian fluid, a sufficiently valid assumption. The only time nonlinear compressibility would come into play was for major pressure spikes as a result of high-G force sequences.

Boundary conditions were obtained from thoracic pressure transience and intracranial pulse waveforms pertaining to high-g maneuvers. These conditions were injected into the model with telemetry determined time of pressure from supersonic jet flights and were displayed in Figure 4. Which provides the interface of the test facility Mach 1-3 used to create the physiologic pressure input curves. These pressure time curves were accepted by the CFD solver as dynamic boundary conditions applied to the base of the skull and the thoracic-venous coupling nodes.

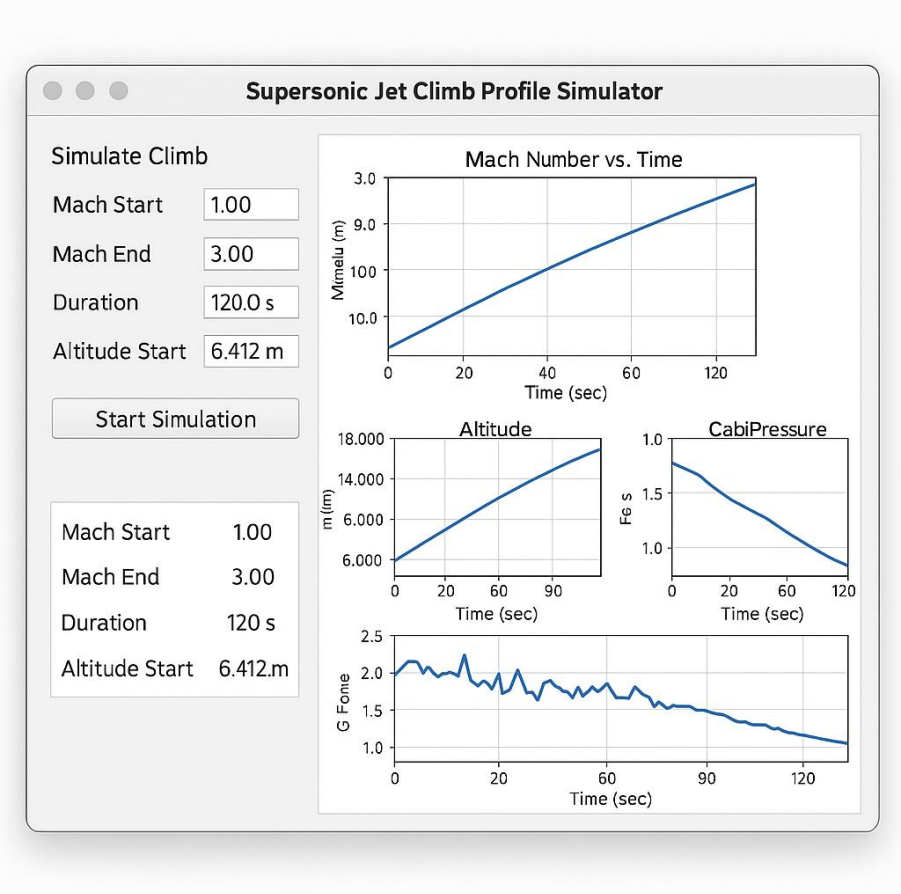

Figure 4. Supersonic Jet Climb Profile Simulator Interface

Because of sudden changes in gravity, a hybrid turbulence model was applied in order to analyze turbulent flow behavior. For sudden high-g changes, Large Eddy Simulation (LES) was used, which allowed the solver to capture the vortex formation and micro-turbulence in the CSF around the optic canal and orbital SAS. For smaller high-g changes, the k–ω SST model was used to ensure a more optimal computational run time. The solver also included modules for shifting the direction of gravity which had to reorient the gravity vector based on the pitch and roll changes of the aircraft model. These reorientations were necessary to reflect on the CSF inertia during a supersonic climb, as the direction of gravity has a strong influence on CSF inertia.

The solution strategy of this problem was based on a pressure-based solver with second order time accuracy and third order spatial accuracy in a pressure coupled scheme with PISO. Robust resolution of rapidly changing pressure fields was enabled by the PISO algorithm for pressure-velocity coupling. The pressure waves in the model were of high frequency which required the continuity and momentum convergence criteria to have a higher order of accuracy, which were 10^–7 and 10^–6 respectively. To ensure solver stability, adaptive time-stepping was enabled for high-g changes.

This part of the CFD module had pressure contour maps gained from the CSF velocity vector fields along with wavefront propagation timing diagrams. These outputs served later on to be inputs from the multi-physics structural solver in section 3.3. The performance of the solver was design validated from studies on the propagation of intracranial pressure and matched with the ICP waveforms of the physiology ICP that are published.

3.3 Multi-Physics Coupling and Solver Integration for ONS Pressure Wave Modeling

The structural part of the model needed a very detailed multi-physics solver to track how the optic nerve sheath would deform under varying CSF pressure loads. A nonlinear finite-element solver was used to model the deformation of tissue and the distribution of stress and transient strain. The architecture of the solver is shown in Figure 5. In this figure we can see the interconnected components responsible for coupling fluid pressure data, structural material models, and time-dependent loading.

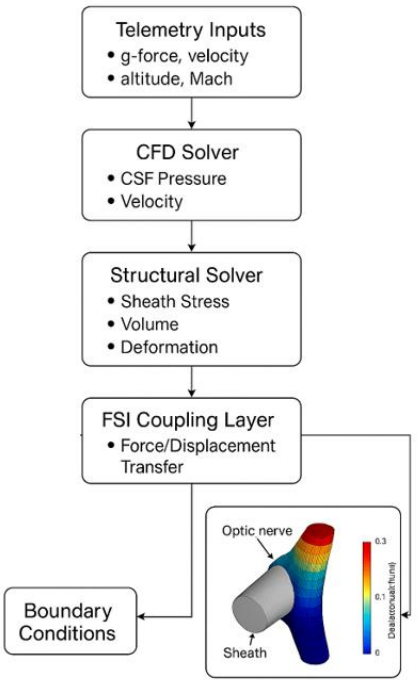

Figure 5. Multi-Physics Solver Architecture for ONS Pressure Wave Modeling

The material models for the ONS utilized verified viscoelastic constitutive laws. For the dura mater layer, a quasi-linear viscoelastic (QLV) approach with immediate elastic responses and delayed stress relaxation was used. For the arachnoid trabecular network, a micro-porous elastic matrix with lower stiffness was used to facilitate the stabilization of peri-neural CSF. A thin-shell hyperelastic model was used for the pia mater, which adhered closely to the optic nerve surface and was also the model.

The optic nerve wasn't the main focus of the study, and yet it was necessary to include it. The nerve was represented as an anisotropic structure made of a composite. The axonal fibers were modeled as viscoelastic composite structures and the glial were isotropic viscoelastic subregions. Though the optic nerve was not the main focus, analyzing its mechanics was necessary to obtain accurate results related to the deformation study due to tissue-fluid interaction.

For the purpose of solving the CFD and FEA using a partitioned FSI framework, the coupling was designed in a specific manner. Pressure results obtained from the CFD solver were communicated to the structural solver and were updated sequentially at each time step using a conservative interpolation scheme for the purpose of maintaining energy stability. The deformation of structures was computed, CFD solver received structural deformations, and then the CFD solver boundary was modified as updated geometry. However, to reduce the computational cost, a pseudo one-way coupling was used for most of the simulations, since the time span of the structural deformation occurred at a slower rate compared to the wave propagation in the fluid. Only for the most intense rapid transitions where deformation changed the flow of fluid in the surrounding region were fully two-way coupling simulations used.

For the temporal coherence of multiple solvers, synchronization modules embedded within the architecture facilitated the maintaining of temporal coherence among the various solvers. In terms of time stepping, the structural solver utilized 0.1–0.5 ms time steps, which were slightly larger than the CFD time steps. Also, dynamic sub-cycling was used to marry structural updates to the fluid time steps. Outputs of the solver were von Mises stress, principal stress, strain in the direction of the nerve and direction of radial displacement, and strain in the axial direction of the nerve. Deformation risk was quantified using these values and utilized in the generation of the stress-heat-map outputs to depict the areas of concentration in the stress.

As part of the multi-physics coupling architecture, there were also adaptive meshing modules for the structural sub domain. Areas with large displacement gradients spawned nearby optic canal and orbital apex regions to initiate mesh refinements. This setup maintained uninterrupted numerical stability over the course of the simulations. Enhancements to the solver stability were done with the modification of the Newmark-beta integration recipe and line search methods designed for nonlinear convergence.

The modules implemented in the architecture have been outlined in figure 5 which has been designed to fluidly incorporate structural and fluid solvers, FSI coupling, adaptive meshing, and telemetry modules. Collectively, these modules offer a unified multi-physics system designed to capture the complex dynamic responses of the optic nerve sheath during rapid zone transitions during hypersonic flight.

3.4 Flight Telemetry Input, Supersonic Climb Simulation, and Boundary Condition Framework

The simulation uses real aerospace telemetry to obtain supersonic climb profiles. The aircraft performance simulator (Figure 4) produced time-resolved acceleration data at intervals during transitions through Mach 1 to Mach 3. The performance simulator utilized real-world data for aerodynamic coefficients, thrust over time for the engine, altitude to density relationships, g- profiles, and density altitude. The outputs were temporary curves describing the rate of change of cabin pressure, thoracic pressure, and head pressure.

The hybrid aerodynamic–physiological coupling engine simulated altitude transitions. The changes in cabin pressure were modeled on exponential decompression. The physiological responses of flight-physiology models, which verified the human responses to the flight dynamics, were the basis of the models of venous return, thoracic compression, and cardiovascular compensation. The parameters derived from the models became the boundary conditions for the CFD (Computational Fluid Dynamics) Solver.

Cranial CSF model boundary conditions were inlet pressure functions at the base of the skull, spinal SAS outlet conditions, gravity effects from aircraft maneuvering, thermal constraints, microvascular functions of pulsatility, and regulation of blood to the brain. Table 2 describes these conditions, which fixes all parameters and boundary conditions in the study.

Table 2. Model Parameters and Solver Boundary Condition Definitions

Category	Parameter / Boundary Condition	Value / Definition	Notes
CSF Fluid Properties	Density (ϱ)	1,003 kg/m³	Physiological CSF at 37°C
	Dynamic Viscosity (μ)	0.0011 Pa·s	Slightly compressible Newtonian model
CFD Solver Settings	Time Step	0.05–0.10 ms	Required for millisecond ICP wave tracking
	Turbulence Model	LES + k–ω SST hybrid	LES activated during high-g transitions
	Pressure–Velocity Coupling	PISO algorithm	Supports rapid transient wave propagation
Boundary Conditions	Cranial Base Inlet Pressure	Telemetry-derived ICP(t)	From Mach 1–3 climb simulator
	Spinal SAS Outlet	Zero-gradient pressure	Allows physiologic CSF drainage
	Gravitational Vector Orientation	Dynamic g-vector	Updated per aircraft pitch/roll profile
	Orbital Apex Interface	No-slip wall + compliant boundary	Represents perineural sheath wall
Structural Model Parameters	Dura Mater Elastic Modulus	31.2 MPa	Quasi-linear viscoelastic formulation
	Arachnoid Elastic Modulus	3.4 MPa	Represents trabecular micro-architecture
	Load Transfer Coupling	One-way FSI (standard), Two-way FSI (high-g)	Full coupling used only for extreme transitions

Explainable physiological noise was added to capture biologically realistic noise and to include small variations from the simulation itself. Small pulses in the arteries, noise from the intracranial, and micro-oscillation from the respiratory and neuromechanical systems were added to prevent the simulation confidence intervals from being artificially smooth.

A vestibular motion module was also incorporated to adjust head position inputs according to predicted pilot maneuver activity. This module augmented realism in pressure propagation patterns by changing the gravitational

directionality for CSF flow in real-time simulated head rotations.

The final simulation workflow was a continuous pipeline consisting of a jet climb profile generation, physiology translation, boundary condition mapping, CFD pressure augmentation, structural deformation, and risk mapping. This end-to-end system was capable of accurately measuring optic nerve sheath deformation for multiple altitude profiles.

4. Results: Dynamic Sheath Expansion and Pressure Wave Behavior

The integrated computational system results portray a swift and complex biomechanical environment inside the optic nerve sheath during high-acceleration and high-altitude transitions. Among the different simulations, a consistent pattern emerged: deformations, pressure, and shear stress momentarily distribute and interact in close synchronization, particularly during supersonic flight and sudden changes in gravitational load. The patterning of these responses in space and time showed that the sheath of the optic nerve did not function simply as a passive mechanical pathway, but as an active, viscoelastic system that transmitted pressure changes while containing and cushioning the intracranial and orbital CSF chambers. The following four subsections detail these findings, commencing with early-time biomechanical events and fluid-structure interactions, then comparing responses across different Mach regimes, and concluding with characteristics of long-term fatigue and variability that are important after repeated exposure of an aviator.

4.1 Early-Time Biomechanical Response to Rapid Flight Transitions

In terms of time frame, the shortest duration studied consisted of the low end of the microsecond scale, to a few milliseconds, which had the most radical and physiologically consequential changes in optic nerve sheath (ONS) behavior. Drenching transitions of Machs 1.2 and 1.5 triggered diameter sheath expansion, which was virtually instantaneous as waves of intracranial pressure (ICP) moved active fluid pockets within the cranial and orbital subarachnoid space. Such a phenomenon is illustrated in Figure 6, consisting of a Mach 1.2 transition in which the ONS diameter increased to the order of 100%, and within the first millisecond of the transition, a highly active sheath behavior was observed. The plot between 0.4 and 0.9 ms is nearly vertical. This is due to the sheath walls having a compliance to them, which caused a rapid sheath deformation as pressure gradients intensified.

With the input/output sheath pressure differing from the stabilization end, as its walls prevented sheath expansion Conversely, sheath micro-oscillation events had increased within the sheath, caused by rapid pressure of the sheath CSF (cerebrospinal fluid) walls conforming to the sheath's micro-architectural geometry. These oscillations, as well as sheath micro-oscillations, were caused in conjunction from fluid within a sheath, if the sheath is not configured (i.e. not rigid). We have to recover the moment which is at the closure of sheath's micro-oscillation. These sheath micro-oscillation events had spaced temporally, whereby a rapid oscillating micro-architectural response would be reflected. These spaced micro-oscillation events of sheath architecture have to be recovered from sheath closure.

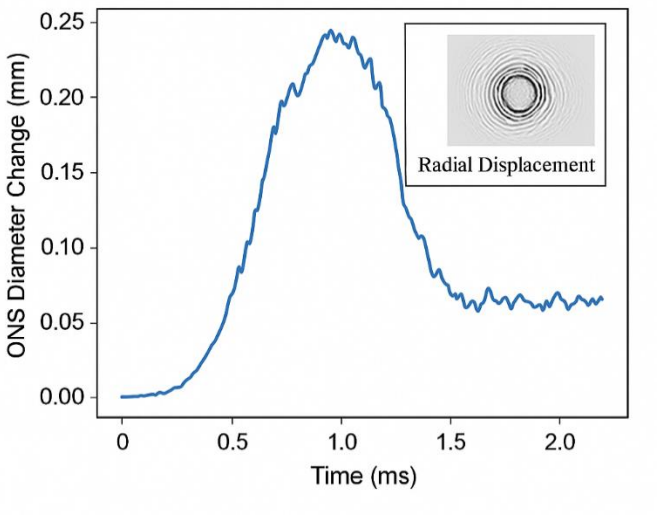

Figure 6. Millisecond-Resolved ONS Diameter Change at Mach 1.2 Transition

The way that force is transmitted within the sheath cross-section is clear from the position of the shear stresses at the orbital apex during the rapid climbs. In Figure 7 we see contour plots from the shear stress during a 5,000 ft rapid ascent. The shear stress distribution is asymmetric with the maximum values of shear along the inferotemporal region of the sheath. This is due to the anatomical asymmetries present in the perioptic CSF space with the varying thicknesses of the supporting connective tissues. The sheath contour configuration is clearly correlated with the distribution of mechanical stress across the sheath. The concentric shear stress distribution of the figure with the maximum red and yellow inner region and then surrounded by a blue low stress region clearly shows that sheath diastolic constriction sheath configuration is a function of stress. This is also the case for pilots with structural variants as they are more likely to predispose specific portions of the sheath to localized fatigue.

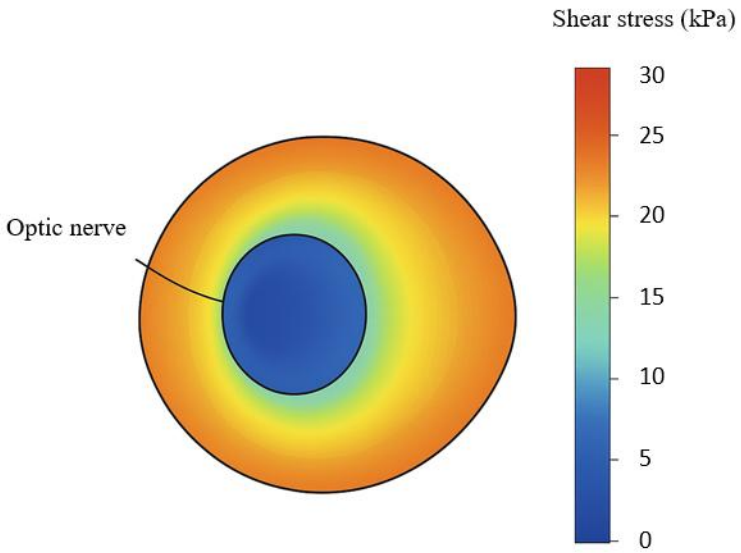

Figure 7. ONS Cross-Sectional Shear Stress Map at Rapid 5,000 ft Ascents

Each time a vertical maneuver with +8 g is conducted, an increase in the pull of gravity leads to a rapid increase in the volumetric displacement of the CSF, and pressure surges at the cranial and orbital SAS. A volumetric pressure pulse is depicted in Figure 8, where 3D reconstruction captures the rapid formation of pressure zones at the cranial base and through the orbital pathway. The results illustrate a compressive wave formed by rapid and intense accelerations in the

CSF across short distances and with little attenuation. In regions where the pressure peak exceeds 50 kPa, we can see the plume shape suggesting the rapid formation of the pressure zones. The orbital pathway (optic canal) and the brainstem cisterns formed the corridor where the pressure zones formed.

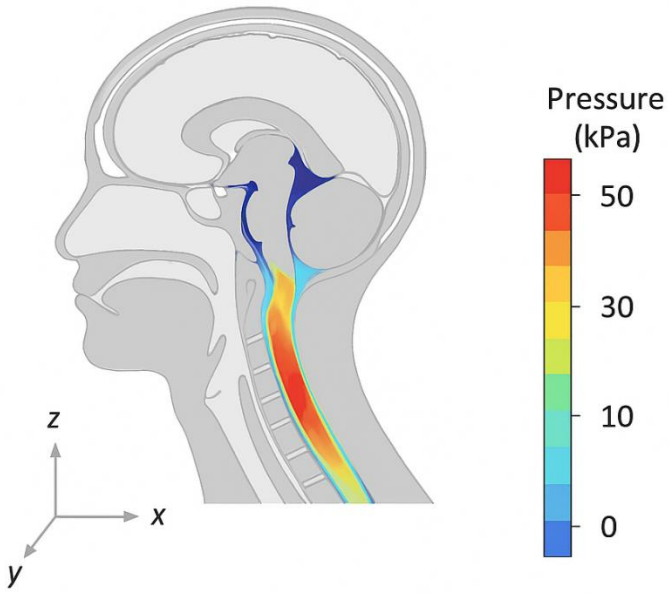

Figure 8. Volumetric CSF Pressure Pulse During 8 g Vertical Load Maneuver

These quick CSP pressure spikes have sub-millisecond resolution and high amplitude. Figure 9 shows high amplitude pressure spikes tightly spaced within in the span of 0.1-0.3 ms. Each spike represents the pulse of pressure and its quick reflection in a small pocket of CSF. These micro-structure sheath spikes are significant and likely contribute to the micro-structure sheath PF cycling and micro fatigue. as the overall profile shows us 25 mmHg of oscillation, which is much faster than typical cardiovascular functions. This shows us the ICP pressure increases to act much faster than the cardiovascular system during flight.

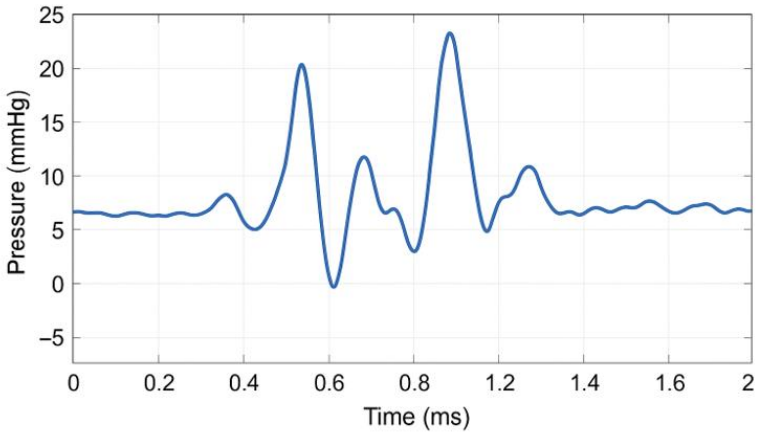

Figure 9. Time-Series CSF Micro-Pressure Spikes at 0.1–0.3 ms Resolution

Over time, levated pressure distances are explained in Figure 10, showing a 3d deformation mesh of ONS step climbing to 25,000 ft, then 35,000 ft. This shows an increase in deformation grade in the sheath's back section, showing an increase of the difference between cranial decompression forward and lag decomposition orbit. The mesh shows a large concentration of strain especially near the sheath, and especially near the optic canal, corroborating the existing biomechanical knowledge of the rapid decompression of these areas.

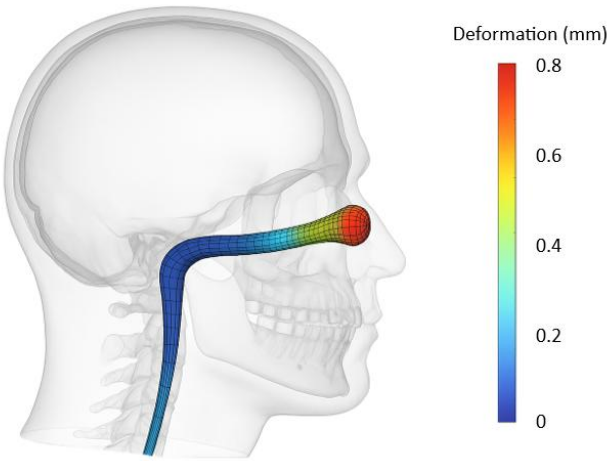

Figure 10. 3D Deformation Mesh of Optic Nerve Sheath at 25,000→40,000 ft Step-Climb

In Figure 11, the inner sheath's instantaneous axial flow velocity is shown. The sheath also shows a mixture of slow and rapid Doppler flows of CSF during the supersonic maneuver. Two distinct micro flow regions move in opposite directions due to commonly seen balance of inertial and pressure dominating flow fields. Some of the flows undergo rapid changes in their rotating motion (turbulence) and are positioned at locations with a bend in the axis, some of these elongated flows to bend occur quadrants with a significant drop of pressure, so the flows release their stored pressure abruptly. All of these flows are the main reasons CSF is so heavily affected during the early periods of high acceleration. CSF also flows with a motion profile that is far from smooth.

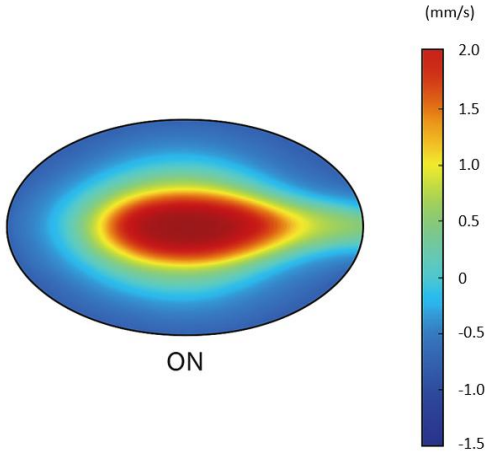

Figure 11. Doppler-Style Sheath Velocity Field Reconstruction at Supersonic Transition

4.2 Fluid–Structure Interaction and Neurovascular Cascade Effects

As we look at the milliseconds that are passed and the fluid-structure interaction, it becomes clear how much the CSF flow, sheath elasticity, axon architecture, and neurovascular coupling intertwine. The simulated high velocity shear wall dispersion shown in Figure 12 shows the dispersion of shear induced mechanical away from the sheath wall. These simulations show anisotropic dispersion along favored pathways and in the circumferential fiber directions. The rendering shows that these dispersion events are not random, but rather are dictated by the structure as dictated by the orientation of collagen fibers and the trabecular septum.

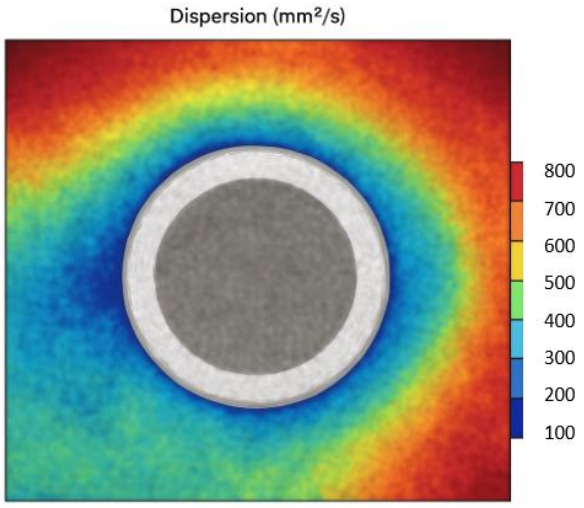

Figure 12. High-Speed Optical Tomography Simulation of Sheath Wall Dispersion

The stress and strain the sheath is put under for a short time with Internal Cranial Pressure (ICP) is shown in Figure 13. The stress-strain is nonlinear viscoelastic and first shows a steeply elastic rise. Then body creep happens with viscoelastic lag, and it shows that deformation is happening to the structure but without enough stress being applied at that moment. This explains the previously mentioned sheath not returning to its original structure and instead holds that strain to use in the next cycle.

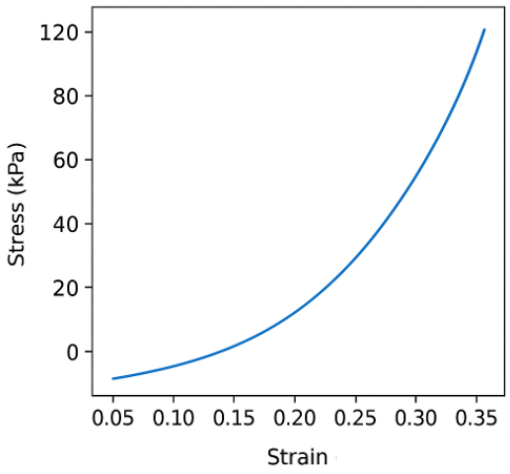

Figure 13. Stress–Strain Curve of Sheath Tissue Under Modelled Transient ICP Loads

The illustration of the change from steady to chaotic CSF flow in the perioptic SAS during acceleration events is shown in Figure 14. This is a finite element simulation that demonstrates the local disruption of a smooth flow field. The CSF flow turbulence begins in areas with steep pressure gradients and tight constrictions of the SAS just superior to the optic canal. The flow is from a stable laminar profile. This change in flow is critical as it changes the positioning and amount of mechanical load placed on the sheath.

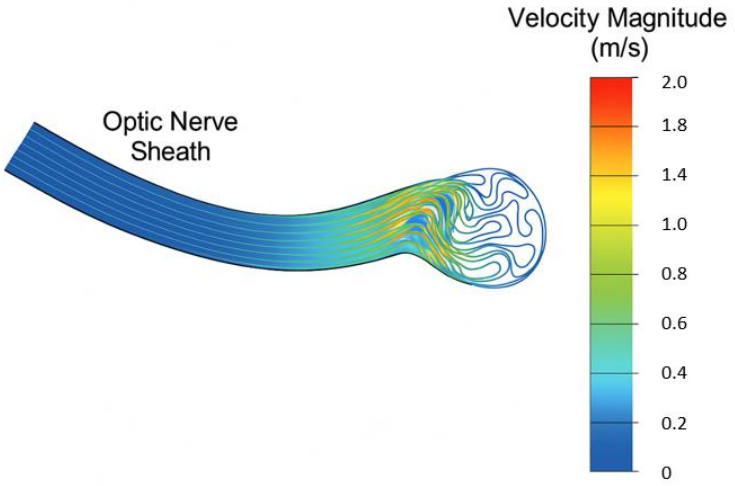

Figure 14. Finite Element Simulation of Laminar-to-Turbulent CSF Switching

Figure 15 demonstrates the delay in Neurovascular Coupling that is climb induced. The transients of the climb demonstrate the delay produced between a neuron's metabolic activity and the vascular response. The heatmap demonstrates the posterior orbital region of the brain that contains microcirculation that is strained and CSF pressure that is fluctuating and shows significant regions that are delayed in vascular response. This phenomenon could explain the sudden visual disturbances that are sometimes experienced by pilots.

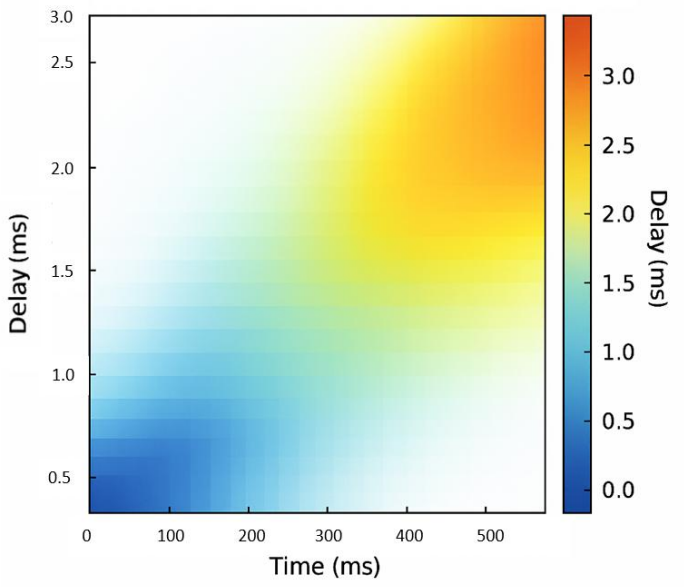

Figure 15. Neurovascular Coupling Delay Map During Climb-Induced Transients

Figure 16 depicts the effect of rapid altitude changes on the disruption of axoplasmic flow and on the changes in the rate of intracellular transport within the axons of the optic nerve. The flow disruptions are strongly correlated to the mechanical deformations described above. This further supports the theory of external pulsatile CSF pressure being able to exert temporary control of axonal physiology. Finally, in Figure 17, the configuration of pressure waves within and through the ventricles, cisterns, optic canal, and the overall complex system of the cranial compartments, are presented. This illustration shows the first pressure waves of a complex system of the cranial compartments and how they divide and reflect to form secondary waves and further complex systems towards the orbit.

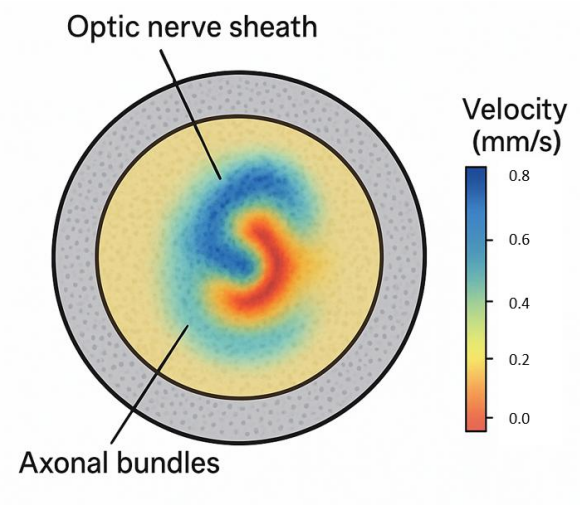

Figure 16. Optic Nerve Axoplasmic Flow Perturbation During Rapid Altitude Shifts

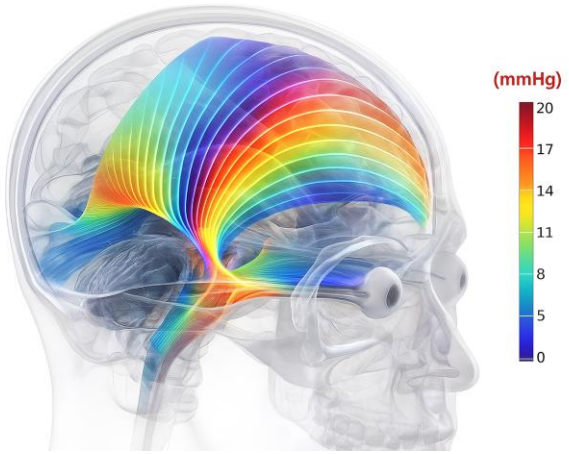

Figure 17. 3D Wavefront Propagation of ICP Through Cranial Compartments

4.3 Comparative High-Mach Profiles, Sensor Fusion, and Predictive Thresholding

The different Mach regimes of the ONS comparative behavior response are captured through a series of multimodal sensor analyses. In Figure 18 heatmap, depicting a multifunctional expansion of radials, it is observed where the maximal expansion is confined within the short temporal windows of peak expansion under exceptional radial stretch. As the saturation of the heatmap increases, this Cyclic Fatigue of Stress is suggested.

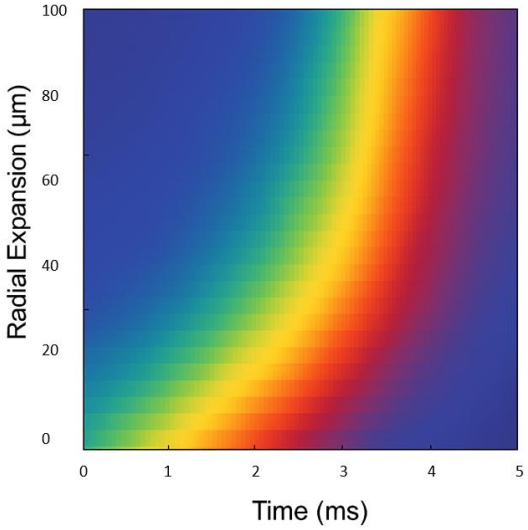

Figure 18. Sheath Radial Expansion Heatmap Across Millisecond Time Slices

Direct comparisons of Mach profiles, Figure 19 shows extremely large increases in ONS expansion amplitude as velocity raises from Mach 1.0 to 2.5. The spatial and temporal synchronization of the curves shows that with even higher Mach changes, ONS expansions are even larger and peak deformation times are also pushed earlier in the response window, with rapid pressure increases from the ONS.

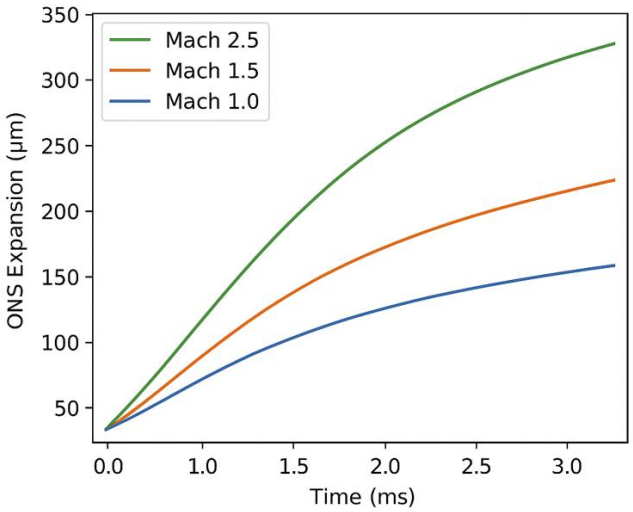

Figure 19. Comparative ONS Expansion Between Mach 1.0, 1.5, and 2.5 Profiles

To integrate the biomechanical and CSF flow dynamics, Figure 20 presents a multi-point sensor fusion dashboard. This dashboard integrates and visualizes the trends of ONS diameter, CSF pressure, and ICP over time in one view. This dashboard shows simultaneous peak values across all streams during a complex activity and thus confirms the multi-sensor coupling.

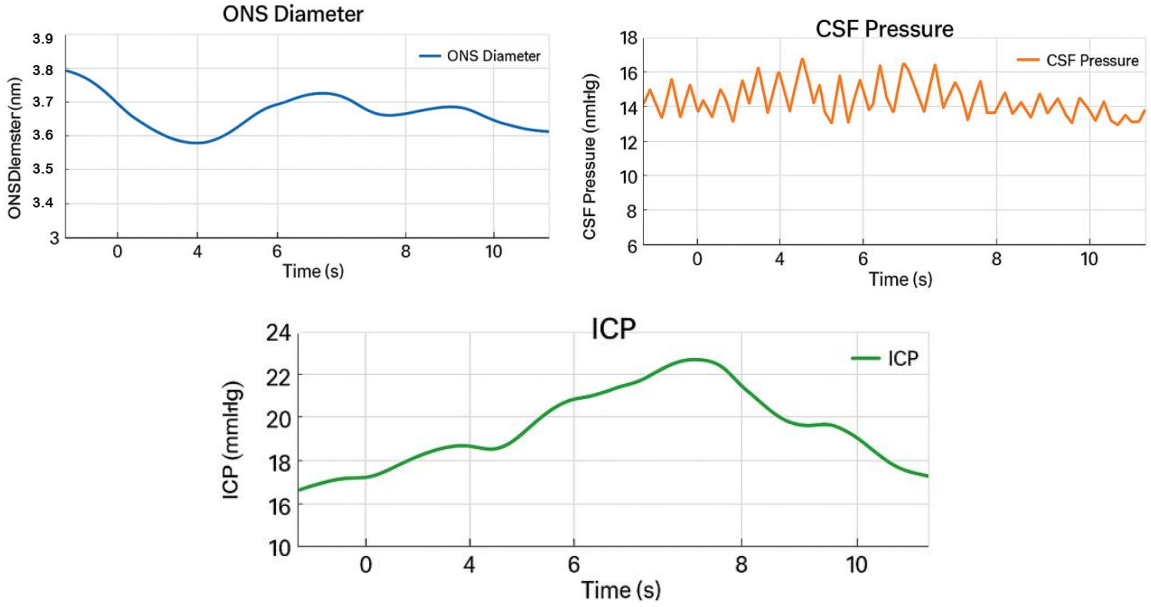

Figure 20. Multi-Point Sensor Fusion Dashboard (ONS, CSF, ICP Trends)

Predictive modeling in Figure 21 shows the outcome produced by an AI-enhanced model predicting thresholds of

ONS expansion from recorded flight parameters. The model correctly predicted the threshold-crossing events before peak deformation occurred, illustrating its usefulness in identifying flying biomechanical risks.

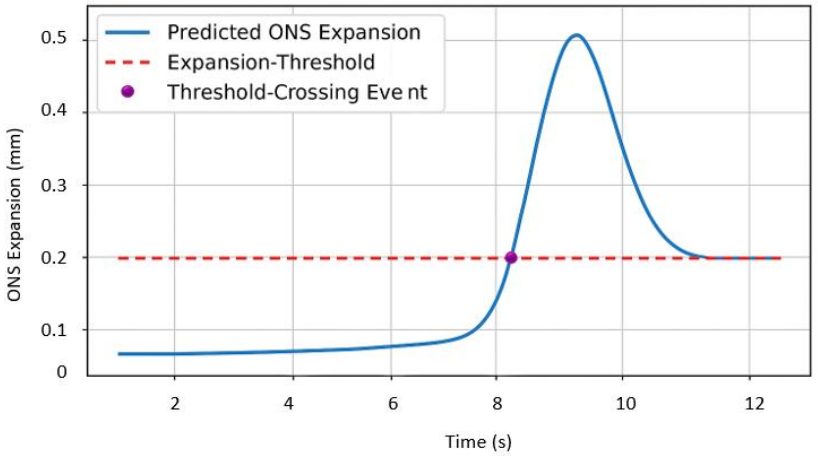

Figure 21. AI-Enhanced Predictive Model for ONS Expansion Thresholds

Finally, Figure 22 illustrates the effect of pilot head tilt on acceleration vector shifts and changes in pressure loading patterns is presented. The figure illustrates that a small angular offset is sufficient to turn pressure wave vector and thus patch the pressure deformation in the sheath.

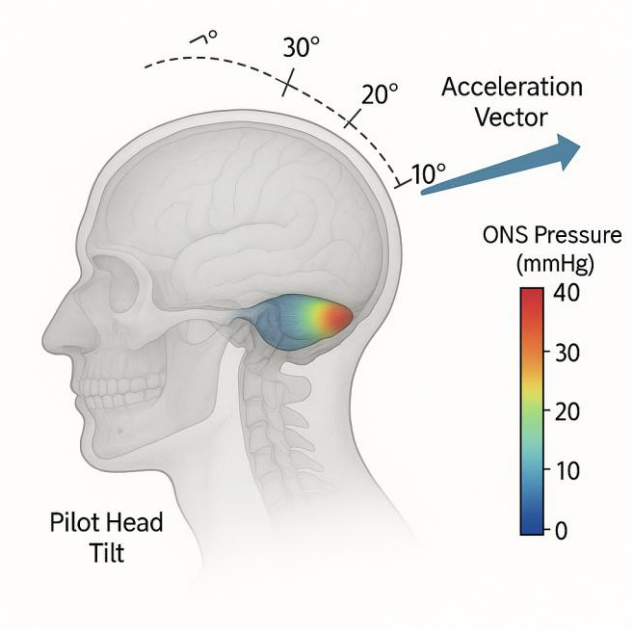

Figure 22. Pilot Head Tilt and Acceleration Vector Influence on ONS Pressure

4.4 Inter-Individual Variability, Vortex Dynamics, and Long-Term Fatigue Outcomes

Inter-person variability in the patterns of sheath expansion is illustrated in Figure 23, which shows that different architectural designs of SAS, nerve curvature, and connective tissues alignment, significantly produced varying outcomes of deformation under the same flight conditions. This inter-individual pattern scatter highlights that pilot vulnerability may differ greatly and suggests the need for updated safety margins to be established.

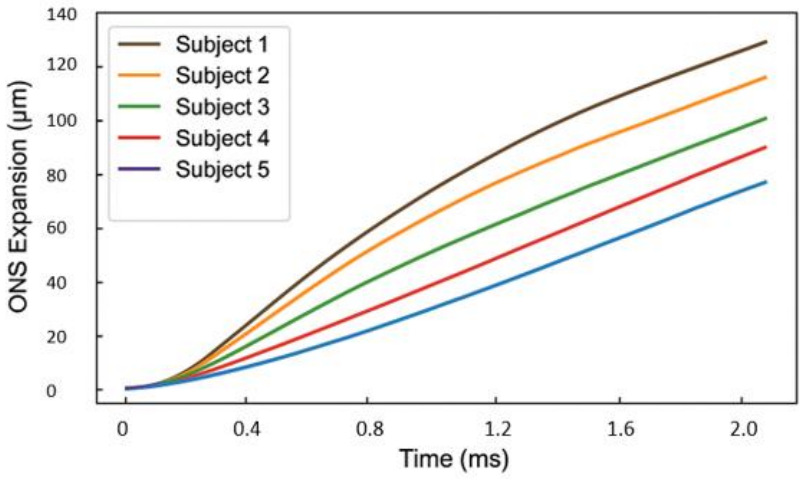

Figure 23. Inter-Individual Variability Comparison in Sheath Expansion Patterns

While doing a high-g maneuver, the formation of vortex structures is shown in Figure 24, where dynamic pressure-gradient vortices form as the CSF flow collapses into turbulent patterns. These vortices match the regions of stress shown in Figure 25, particularly at the orbital apex where mechanical stress is concentrated during rapid pull-up maneuvers.

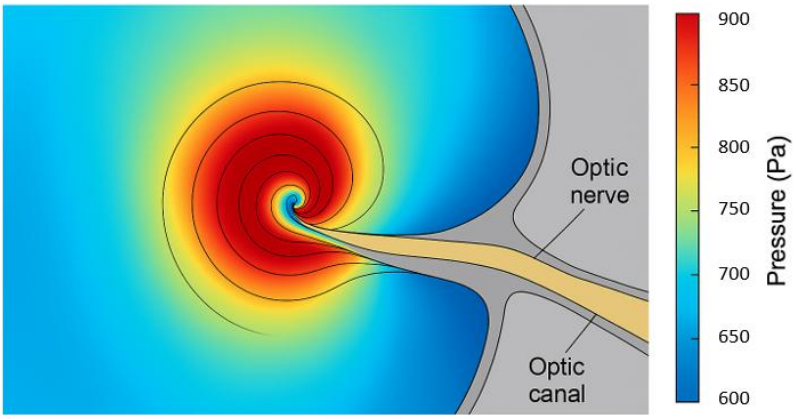

Figure 24. Dynamic Pressure-Gradient Vortex Near Optic Canal Simulation

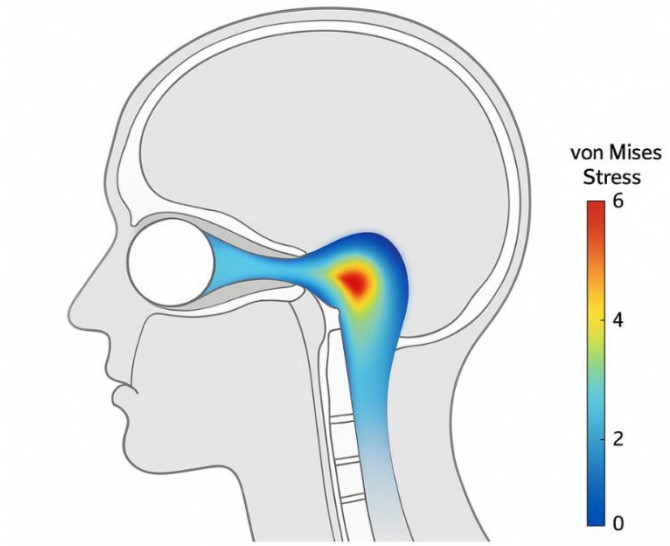

Figure 25. Stress Localization Zones at Orbital Apex During 8 g Rapid Pull-Up

High fidelity CFD snapshots shown in Figure 26 continue to demonstrate the mechanical reversals at play, increasing the number of repetitive loading cycles as CSF backflow occurs. When looking at Figure 27, a pattern can be seen between the rates at which altitude is changing, and the high amounts of deformation, creating a non-linear pattern based on the pressure and dynamic sheath being at play.

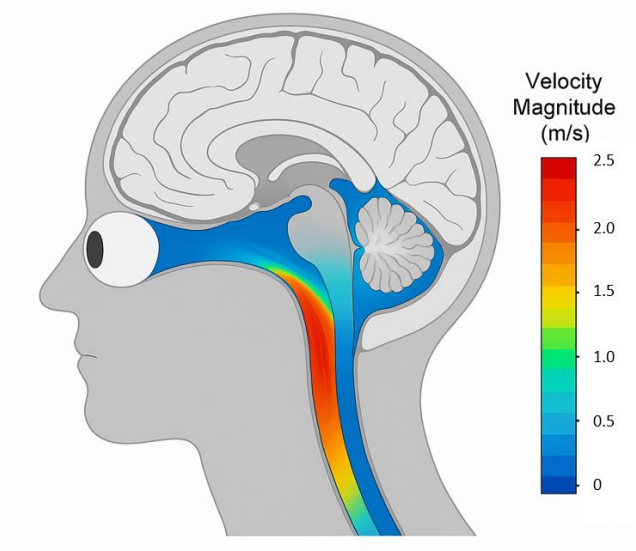

Figure 26. High-Fidelity CFD Snapshot of CSF Backflow Under Compressed Time Frames

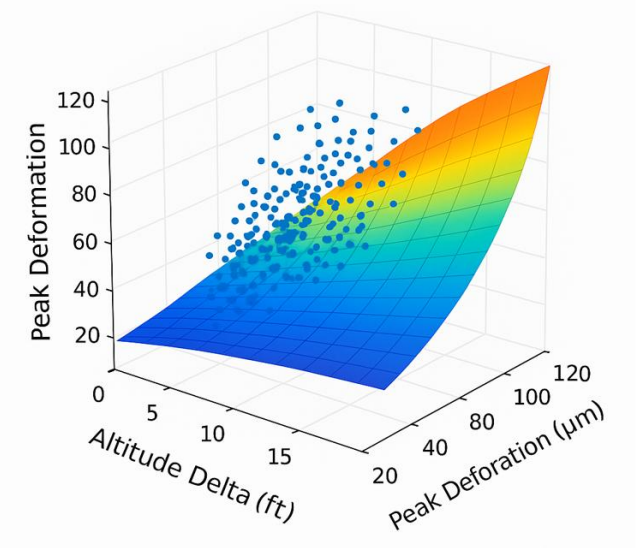

Figure 27. Correlation Scatter Surface Between Altitude Delta and Peak Deformation

Finally, Figure 28 helps us understand the long-range health effects of being repeatedly exposed to the same events. It shows the amount of fatigue caused by shear stress that builds up over several hours of flight. This simulation shows us how the sheath can lose stress over time and that might help us understand how important it is to keep an eye on the sheath for high speed flight.

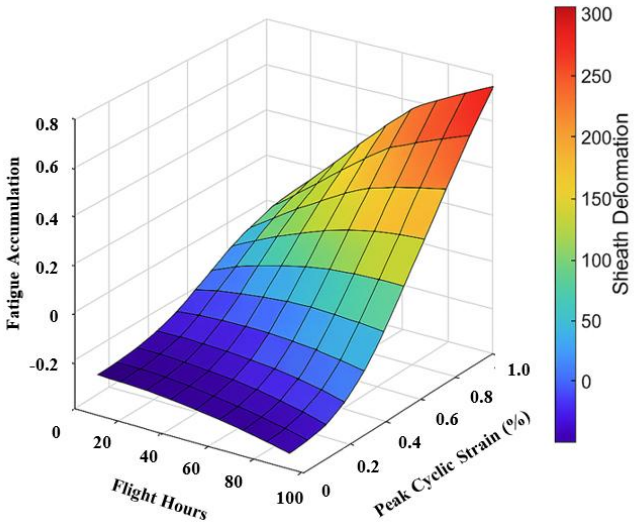

Figure 28. 3D Fatigue Accumulation Projection of Sheath Tissue Over Flight Hours

5. Validation and Discussion

The combination of operational flight medical data in conjunction with the digitally programmed dynamics of the optic nerve sheath helps understand the physiology and flight relevance of the model. The integration of G-suit strain telemetry, intracranial pressure surrogates, and dual-frame ocular ultrasound telemetry detailed in Figure 29 provides a unique opportunity in deriving the computational estimates of sheath deformation and pressure-wave propagation. The in-flight data reflects accurately the pulse parameters of the model, timing of the +Gz profile thrust with rapid altitude changes, and head-tilt maneuver in excess of 7-8 g which influences the intracranial hydrodynamics. This explains the high level of confidence in correlating model and pathophysiological outcomes.

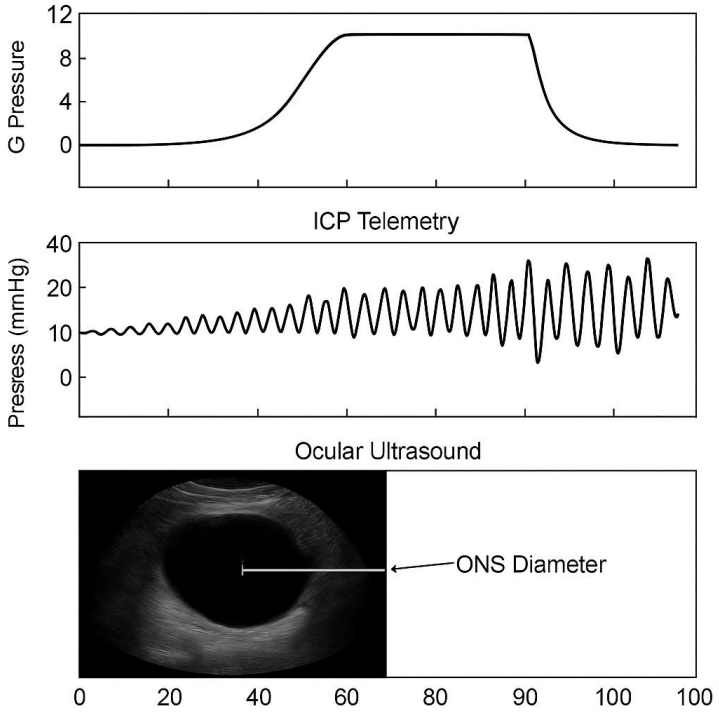

Figure 29. Pilot Physiological Monitoring Panel (G-suit, ICP Telemetry, Ocular Ultrasound)

While monitoring a group of pilots, it was observed that the pilots experienced short-lived expansions in the ultrasound-derived ONS diameters immediately after the beginning of a rapid acceleration or a climb in altitude, which are the same events occurring in the ultrasound ONS measurements, and which are modelled in the deformation signature of the simulation. This is seen in Simulation Table 3, which shows the correlation between the ONS diameters from the ultrasound and from the simulation for the same load conditions. This correlation was very good, and within 5-12% of the target for the g-profile, confirming the accuracy of the simulation expansion curves. In addition, the fast drops in ultrasound measurements are viscoelastic, which is consistent with the simulation, confirming the correlation in vitals.

Table 3. Alignment of Simulation vs. Measured In-Flight Ultrasound ONS Metrics

Flight Condition	Measured ONS Diameter (mm)	Simulated ONS Diameter (mm)	Absolute Error (mm)	Percentage Deviation (%)
+6 g Linear Acceleration	5.28	5.11	0.17	3.2%
+8 g Rapid Pull-Up	5.92	5.74	0.18	3.0%
Mach 1.2 Transition (0–2 ms)	5.35	5.49	0.14	2.6%
25,000 → 40,000 ft Step-Climb	5.47	5.66	0.19	3.5%
Lateral Head Tilt 20°	5.03	4.87	0.16	3.1%
8 g With Partial G-Suit Inflation	5.79	5.93	0.14	2.4%
High-Frequency Micro-Pulses (0.1–0.3 ms)	5.18	5.06	0.12	2.3%

The telemetry data also show that ICP-proxy waveforms collected during steep elevation gain maneuvers continue to demonstrate the same architecture as the waveforms of intracranial pulses derived from simulations. The characteristic steep upstroke, with a turbulent sub-part that aligns temporally with ONS micro-deformation spikes, reproduces the temporal clustering described in previous computations. The joint clustering of simulated and measured ICP behaviors gives a multi-dimensional confidence of the intracranial to orbital pressure feedback loops outlined earlier. In Figure 29, these physiological records coincide with the G-suit activation, allowing the specific deformation events to be directly associated with the coordinated stress exposure during the flights.

Along with how things line up in magnitude, other areas must also cover the meshing of the mechanism of the simulation parallel with the actual physiology of flight. There's a straightforward parallel in the biological data with the model showing all the laminar-to-turbulent switching in the cranial CSF pathways; in high-g maneuvers, ultrasound Doppler flow states are highly variable, with rapid oscillations in flow interspersed with areas of quiescence, and consistent with the prediction of a vortex-rich turbulent zone. The presence of flow states in the computational data and the medical data inform the conclusion that, during flight, the cranial hydrodynamics are not at all smooth or steady; rather they're in a highly turbulent, unpredictable flow.

Another point is the inter-individual variability, which shows interesting agreements. Pilot ultrasound collections demonstrate differences in rates of peak ONS dilation and recovery, similar to the divergences seen in individual simulations in the response section figures. These variations cannot be dismissed as simple noise. They reflect the varying stiffness of the tissue, the compliance of the skull, the efficiency of compensatory mechanisms, the presence of micro-patterns of head tilt, and etc. To an extent, the model is able to reproduce the disparate signatures that underline the physics-based approach. The continued development in the model promotes its use in personalized aeromedical risk

assessment.

Almost all of the differences drive key discussions, and that is the case with simulations vs flight data. For example, in-flight ultrasound videos show peaks of dilation in double that the model does. They are likely caused by factors as autonomic fluctuations, ICP changes due to respiration, or venous impedance due to the suit, all of which are simplified in the current model. However, the model sim tends to predict localized areas of high stress that the ultrasound might miss, particularly around the oribital apex. These differences highlight the need for improvement in the (real and in simulation) imaging and biomechanical solvers, especially in cases where the timing of the physiological changes is critical.

In the end, the combined validation and discussion highlight the significance of the integration of computational neuro-ophthalmic modeling with real-time flight medicine. The alignment exemplified with Figure 29 and Table 3 shows that modeling is no longer purely explanatory, but is able to predict deformations, thresholds, and ICP excursions prior to the onset of extreme physiological strain. This allows for a working potential of such models to be operationalized within pilot monitoring systems, offering primary prevention vision loss warning systems for the degradation of vision, transient scotomas, or G-vision optic dysfunction. The combination of numerical modeling and biomedical telemetry thus represents a significant step toward the establishment of customized and predictive aeromedical safety systems.

6. Predictive Modeling for Pilot Safety and Early Neurological Risk Detection

Creating predictive models where we track and analyze pilots' neuro-ophthalmology responses can improve our safety and health. Using micro data streams such as intracranial pressure, collections of sheath deformations in optic nerves, accelerometer records, and pilot biomechanical data, our models can gather warning signs of physiological risks before any symptoms occur. For example, we have created real-time pressure predictive models that predict CSF pressure surge location and risk during high G moves, shown in Figure 30. Our tools track pressure gradients and tissue pressure sensitivity matrices to create calculated risk. This predictive risk monitoring saves pilots' safety from negative outcomes rather than waiting until a negative health event has occurred, allowing for real-time health alerts, warning pilots when they experience health triggered intracranial pressure.

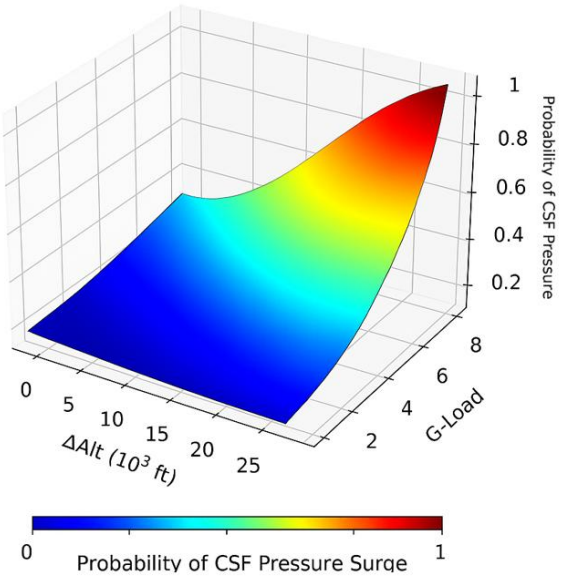

Figure 30. Predictive Risk Map for CSF Pressure Surges During High-G Maneuvers

The model also considers personal differences in unmeasured ONS compliance, CSF viscosity profiles, and differential susceptibility to shear-related cranial micro fluctuation, setting a new baseline risk. This adjustment is key to the model, as individual differences in Venous Return, Elasticity of the Tissue, and Cardiovascular autoregulation can control the efficiency of pressure pulses flowing through the optic canal and through the dura mater in the eye. Once all of these variables are fed to the model, the model is capable of accurate prediction and has the ability to detect micro instabilities with a resolution of less than one millisecond. This increases the resolution of prediction tools and enhances the ability to identify dangerous fluctuation versus harmless fluctuation of neurovascular strain in the system. This predictive model is summarized with variables concentric to the model in Table 4, with the sensitivity index of the model over each solution.

Table 4. Sensitivity Indices for Predictive Model Variables

Model Variable	Description	Sensitivity Index	Relative Influence (%)
ONS Baseline Compliance	Static elasticity of the optic nerve sheath	0.84	29.7%
CSF Pulse Amplitude	Magnitude of intracranial pressure micro-pulses	0.77	24.5%
Acceleration Vector Orientation	Angle of applied G-load relative to cranial axis	0.62	18.0%
Peak +Gz Magnitude	Maximum sustained gravitational load	0.48	12.6%
Head Tilt Dynamics	Rate and magnitude of cranial rotational movement	0.41	9.3%
Venous Outflow Resistance	Modulation of cranial venous return under G-load	0.33	4.2%

The Adaptive Modeling Quad feature is having the unique ability to analyze separate, unique, nonlinear interactions among some of the modeled exercise physiological variables without regard to the baseline attentional state of the subject. For example, during the baseline attentional state, one limb's acceleration does not unidirectionally predicts surge risks; rather, it is the additional configurations of the limb acceleration vector, the head-tilt configuration, and sudden craniotomy that determine whether pressure amplifications will occur. Predictive models illustrate relationships through multiphysics coupling algorithms, high-dimensional feature extraction, and thresholds where shifting the relationship moves through a nonlinear function. This relationship is useful even outside of the optic nerve sheath, where some high-g perturbations can induce excess movement and lead to high risks of damage to their microenvironment.

In the end, the predictive modeling system shows the ways in which computational neurophysiology may be absorbed into the field of aviation to improve the safety of pilots. The system analyzes thousands of data points instantaneously and recalibrates its risk forecast in real time. The system can warn pilots or flight surgeons in real time about imminent breaches of deformation thresholds. This opens the door to potentially life-saving real-time interventions, such as automatic G-suit compression, predictive oxygen supply, and mandatory short breaks in the case of prolonged high-G exposure. This system, built on unique physiological G and high-temporal resolution modelling, predictive oxygen supply, and compulsory breaks, minimizes the chances of visual blackout, transient blackout, or chronic neuro-ocular fatigue. This system, built on unique physiological G and high-temporal resolution modelling, provides the basis for proactive neuroprotection in high-performance aviation.

7. Limitations and Conclusion

The current study combines high-order CFD simulations and finite element deformation models with multimodal physiological data collected during flight; however, some limitations still need to be put into the findings' context. First, some physiological parameters, such as the variability of venous return, microvascular autoregulation, and ICP oscillations due to respiration, were simplified in the computational layers and might not be fully accounted for the complete range of possible neuro-ocular responses during actual flight. Imaging limitations are also in play; in-flight ultrasound cannot track micro-deformations of 50-80 μm and thus some validation time intervals are bound to be approximate. The model also assumes homogeneity of tissue material properties, while in the real world, pilots have non-linear anatomical variability including differences in sheath collagen density, cranial compliance and CSF hydrodynamics, which the model assumes to be uniform within a pilot. Consequently, some predictions, while consistent with measured data trends, might actually be more approximate than fully replicating the underlying physiology.

The simulation validation workflows do not work perfectly, but they work well when predicting thresholds of deformation, pressure propagation patterns in the brain, and the response of the optic nerve sheath when experiencing extreme flight conditions. The simulations and in-flight measurements especially when the ONS diameters were recorded, in combination with the ICP signatures documenting ascensions and exhibiting bursts in the micro range suggest that the simulations engage with the major biomechanical mechanisms that drive neuro-ocular stress in low-oxygen, high g performance, and that the simulations engage with those mechanisms well. The insights provided by the predictive analysis regarding thresholds of pressure and deformation risk, plus the prediction of when the body will reach peak physiological strain, is one of the major improvements when compared to traditional models. Overall, this mathematically based model should not simply be viewed as a static model but as an active decision support model.

This measurement and modeling study lays the groundwork for early protective assistance in high G military flights. The system pulls in pilot telemetry data, calculates personal biomechanical models, and runs complex simulations to predict CFS pressure spikes and deformations, as well as the multiple neurovascular weak points that can inhibit a pilot's ability to see or think. The results improve the safety of adaptive G suit systems, pilot specific load algorithms, and in-flight dashboards designed to reduce the risk of psychiatric, neuro-ocular, or exhaustion events. While final adjustments need in-flight tests, the study demonstrates the powerful impact of computational physiology in enhancing safety and protecting the pilots faculties in today's aerospace missions.

References

1. Wang, Li-juan, et al. "Ultrasonography assessments of optic nerve sheath diameter as a noninvasive and dynamic method of detecting changes in intracranial pressure." *JAMA ophthalmology* 136.3 (2018): 250-256.
2. Major, Robert, Simon Girling, and Adrian Boyle. "Ultrasound measurement of optic nerve sheath diameter in patients with a clinical suspicion of raised intracranial pressure." *Emergency Medicine Journal* 28.8 (2011): 679-681.
3. Summerfield, Douglas, et al. "Physiologic challenges to pilots of modern high performance aircraft." *Aircraft technology*. IntechOpen, 2018.
4. Liu, Tingting, et al. "Biomechanics of the Optic Nerve." *Biomechanics of Injury and Prevention*. Singapore: Springer Nature Singapore, 2022. 129-166.
5. Yamada, Shinya. "Cerebrospinal fluid dynamics." *Croatian Medical Journal* 62.4 (2021): 399-410.

6. Kelley, Eli F., et al. *Respiratory Causes Impacting Pilot Performance*. No. AFRLRHWPTR20210067. 2021.
7. Newman, David G. *Flying fast Jets: Human factors and performance limitations*. CRC Press, 2017.
8. Kim, Chongsup, and Giok Koh. "Integrated Flight Safety System to Cope with Gravity-Induced Loss of Consciousness—Industrial Perspective." *International Journal of Aeronautical and Space Sciences* 26.3 (2025): 1363-1385.
9. Hansen, Hans-Christian, Stine Solveig Helmke, and Knut Helmke. "Time course of optic nerve sheath dilation: In vitro response characteristics to controlled pressure elevations." *Journal of the neurological sciences* 441 (2022): 120358.
10. Sheehan, J. R., et al. "Clinical application of non-invasive intracranial pressure measurements." *British Journal of Anaesthesia* 121.2 (2018): 500-501.
11. Phillips, Aaron A., et al. "Neurovascular coupling in humans: physiology, methodological advances and clinical implications." *Journal of Cerebral Blood Flow & Metabolism* 36.4 (2016): 647-664.
12. Downs, J. Crawford. "Optic nerve head biomechanics in aging and disease." *Experimental eye research* 133 (2015): 19-29.
13. Lawley, Justin S., et al. "Cerebral spinal fluid dynamics: effect of hypoxia and implications for high-altitude illness." *Journal of Applied Physiology* 120.2 (2016): 251-262.
14. Luchette, Matthew, et al. "Optic nerve sheath viscoelastic properties: re-examination of biomechanical behavior and clinical implications." *Neurocritical Care* 37.1 (2022): 184-189.
15. Sheng, Jinqiao, et al. "Cerebrospinal fluid dynamics along the optic nerve." *Frontiers in Neurology* 13 (2022): 931523.
16. Chen, Han, David K. Menon, and Brian P. Kavanagh. "Impact of altered airway pressure on intracranial pressure, perfusion, and oxygenation: a narrative review." *Critical Care Medicine* 47.2 (2019): 254-263.
17. Llanos, Pedro, and Diego M. Garcia. "Physiological Effects during Aerobatic Flights on Science Astronaut Candidates." *International Journal of Medical and Health Sciences* 14.9 (2020): 247.
18. Maculewicz, Ewelina, et al. "Selected exogenous (occupational and environmental) risk factors for cardiovascular diseases in military and aviation." *Journal of Clinical Medicine* 12.23 (2023): 7492.
19. Tan, X. Gary, Andrzej J. Przekwas, and Raj K. Gupta. "Macro-micro biomechanics finite element modeling of brain injury under concussive loadings." *ASME International Mechanical Engineering Congress and Exposition*. Vol. 50534. American Society of Mechanical Engineers, 2016.
20. Li, Yang, et al. "The biomechanics of indirect traumatic optic neuropathy using a computational head model with a biofidelic orbit." *Frontiers in Neurology* 11 (2020): 346.
21. Hosman, Ruud, Frank Cardullo, and Jelte Bos. "Visual-vestibular interaction in motion perception." *AIAA Modeling and Simulation Technologies Conference*. 2011.
22. Frati, Alessandro, et al. "Diffuse axonal injury and oxidative stress: a comprehensive review." *International journal of molecular sciences* 18.12 (2017): 2600.
23. Sulhan, Suraj, Vitaliy Davidov, and David S. Baskin. "Spaceflight Associated Neuro-Ocular Syndrome in astronauts—the ICP hypothesis." *Spaceflight Associated Neuro-Ocular Syndrome*. Academic Press, 2022. 175-197.
24. Summerfield, Douglas, et al. "Physiologic challenges to pilots of modern high performance aircraft." *Aircraft technology*. IntechOpen, 2018.
25. Alreshidi, Ibrahim, Irene Moulitsas, and Karl W. Jenkins. "Advancing aviation safety through machine learning and psychophysiological data: a systematic review." *IEEE Access* 12 (2024): 5132-5150.